Revista Brasileira de Cartografia
ISSN 1808-0936 | https://doi.org/10.14393/revbrascartogr
Sociedade Brasileira de Cartografia, Geodésia, Fotogrametria e Sensoriamento Remoto

# Water Level Dynamics in Rio Grande City (RS) During the Major Flood of May 2024 Assessed Using a GNSS-R Sensor and Conventional Tide Gauges

*Dinâmica do Nível da Água na Cidade de Rio Grande (RS) Durante a Grande Cheia de Maio de 2024: Comparação entre Sensor GNSS-R e Marégrafos Convencionais*

Manuella Anaís Rodrigues Fagundes [1] and Felipe Geremia Nievinski [2]

1Federal University of Rio Grande do Sul, Porto Alegre, Brasil. manuella.fagundes@ufpe.br
Federal University of Pernambuco, Recife, Brasil.
ORCID: https://orcid.org/0000-0003-3447-8582
2 Federal University of Rio Grande do Sul, Porto Alegre, Brasil. felipe.nievinski@ufrgs.br
ORCID: https://orcid.org/0000-0002-3325-1987

Recebido: 03.2025 | Aceito: 04.2025

**Abstract:** The city of Rio Grande (RS) was partially flooded in May 2024, when an extreme weather event significantly increased the water level of the Patos Lagoon. In this context, we analyzed the water-level dynamics in the Rio Grande estuary during the event by comparing data obtained from a reflectometric tide gauge based on navigation satellites (GNSS-R) with measurements from five conventional tide gauges: a staff gauge, three radar sensors, and a pressure sensor. The comparison between the GNSS-R sensor and the co-located staff gauge showed a strong coefficient of determination (0.99) and a centimeter-level standard deviation (3.8 cm). In contrast, the comparison between the GNSS-R sensor and the most distant gauge (20 km) resulted in a lower coefficient of determination (0.6) and a decimeter-level standard deviation, because of the spatial variability in water level between the estuary and the breakwater region. To better understand the water-level dynamics, a harmonic analysis was conducted considering the main diurnal tidal constituents, K1 and O1. The harmonic analyses highlighted the complexity of the water-level dynamics in terms of amplitude and phase. Finally, the results indicated a strong coefficient of determination between the GNSS-R measurements and those of the conventional sensors, demonstrating that agreement is inversely proportional to the distance between sensors.
**Keywords:** GNSS-R altimetry. Water level dynamics. Tide Gauges.

**Resumo:** A cidade de Rio Grande (RS) foi parcialmente inundada em maio de 2024, quando um extremo climático elevou significativamente o nível da Lagoa dos Patos. Diante deste cenário, analisamos a dinâmica do nível da água no estuário de Rio Grande durante o evento, comparando dados obtidos por um marégrafo refletométrico baseado em satélites de navegação (GNSS-R) e por cinco marégrafos convencionais: uma régua, três sensores radar e um sensor de pressão. A comparação entre o GNSS-R e a régua, coincidentes espacialmente, demonstrou forte coeficiente de determinação (0,99) e desvio padrão centimétrico (3,8 cm). Já a comparação entre GNSS-R e o sensor mais distante (20 km) resultou em um coeficiente de determinação menor (0,6) e desvio padrão decimétrico, como consequência da variabilidade espacial no nível da água entre o estuário e a região dos molhes. Para melhor compreender a dinâmica do nível da água, foi realizada uma análise harmônica, considerando as principais constituintes diurnas de maré, K1 e O1. As análises harmônicas apontaram a complexidade da dinâmica da água na região em termos de amplitude e fase. Por fim, os resultados indicaram um forte coeficiente de determinação entre as medições do sensor GNSS-R e dos sensores convencionais, apontando que a concordância é inversamente proporcional à distância entre os sensores.
**Palavras-chave:** Altimetria GNSS-R. Dinâmica do nível da água. Marégrafos.

## 1 INTRODUCTION

Since the 18th century, Rio Grande (RS) city has developed in close connection with the Patos Lagoon and the Atlantic Ocean (Torres, 2012). Historical records document rising water levels and extreme weather events, such as the Great Flood of 1941. With the worsening effects of climate change, the need to mitigate damage and ensure public safety has become increasingly urgent. In this context, accurate water level

measurements are essential for forecasting flows, delineating risk areas, and designing appropriate infrastructure (Marques & Möller, 2008; Nogueira, 2006; Oliveira, 2008).

Visual/manual staff gauges and automatic water level sensors have been widely used to monitor variations in water level. Among conventional tide gauge instruments, hydrostatic pressure sensors and radar altimeters are particularly noteworthy. These devices operate below or above the water surface, respectively, making them vulnerable to damage under atypical water level fluctuations. Their installation requires both logistical and technological planning, and their accuracy depends on sensor placement and routine maintenance. Furthermore, it has been widely reported that conventional sensors are often subject to theft, vandalism, or complete destruction, rendering them inoperative during extreme events (Carrillo, 2024; Geremia-Nievinski et al., 2024; Marcuzzo et al., 2024).

Considering this scenario, Global Navigation Satellite System Reflectometry (GNSS-R) has emerged as an innovative and promising alternative for water level monitoring. GNSS-R is based on the bistatic radar principle, in which the receiver and transmitter are spatially separated. It employs radio waves emitted by navigation satellites to perform remote sensing of the Earth's surface (Larson, 2016). This technology has been applied to monitor water levels in coastal and riverine environments (Holden & Larson, 2021; Larson et al., 2017; Purnell, Gomez, Minarik, & Langston, 2024). Operating GNSS-R sensors from shorelines - at a safe distance from the sea, rivers, lakes, or reservoirs - enhances the resilience of the system to waves and flooding, which frequently damage conventional instruments.

In May 2024, the state of Rio Grande do Sul experienced widespread severe flooding that led to the failure or loss of conventional water level sensors in the Guaíba basin. In this study, we analyzed the water level dynamics in the city of Rio Grande during the May 2024 flood. All available tide gauges in the municipality were utilized, including one GNSS-R sensor and five conventional instruments. This work aimed to assess the applicability of GNSS-R technology, specifically through an open-source sensor developed by Fagundes, Tinti, Iescheck, Akos, and Nievinski (2021), later enhanced by the startup TideSat (Fagundes et al., 2021), under extreme weather conditions. Additionally, we investigated the hydrodynamic behavior of the estuarine system by analyzing both the astronomical and meteorological components of the tide at different sites across the city. Through this investigation, we aim to support strategic planning actions to improve local resilience.

In the following sections, we briefly review the theoretical foundation of the techniques employed. We then describe the methodology adopted in this experiment. Numerical and graphical results are presented and discussed. Finally, we conclude the study with key findings and suggestions for future work.

## 2 BACKGROUND

### 2.1 Traditional Tide Gauge Monitoring

The Intergovernmental Oceanographic Commission provides detailed guidelines for sea level monitoring, encompassing all stages from planning to the installation and maintenance of tide gauges. The Sea Level Manual (2006), published by the Commission, emphasizes the necessity of redundancy and establishes that at least two sensors are required to ensure data continuity. Similarly, it underscores the need for a GNSS receiver installed as close as possible to the tide gauge to monitor its position (IOC, 2006).

In many applications, such as climate studies, long-term time series are essential. However, in Brazil, only two stations possess records exceeding fifty years in duration (PSMSL, 2019). The fluvial monitoring context faces the same challenges common to all monitoring systems, including theft and vandalism. Addressing such vulnerabilities demands redundancy at each installation site to guarantee data collection over extended periods.

Conventional automatic measurement technologies, such as pressure sensors and radar, present challenges related to high installation and maintenance costs and are susceptible to failures during extreme events. For instance, pressure tide gauges may require divers for installation, while radar sensors necessitate appropriate supporting structures. The staff gauge, the most common and low-cost option, can be inefficient under extreme conditions such as droughts and floods. Additionally, the diversity of equipment complicates maintenance, requiring skilled personnel for calibration and adjustments. Although conventional instruments

exhibit high accuracy, all methods are subject to systematic and random errors. Factors such as support structure vibration and adverse weather conditions can affect radar measurements, whereas pressure tide gauges are sensitive to water density and sedimentation (IOC, 2006; Míguez et al., 2012).

## 2.2 GNSS REFLECTOMETRY

GNSS reflectometry (GNSS-R) is a method that enables the estimation of environmental parameters surrounding a GNSS antenna (Larson, 2016). It employs an antenna and a receiver to capture radio waves emitted by global navigation satellites. When applied from ground-based platforms (rather than airborne or orbital), the most common GNSS-R modality is known as GNSS Interferometric Reflectometry (GNSS-IR). This technique relies on analyzing interference patterns, constructive or destructive, in the observable signal-to-noise ratio (SNR). These patterns result from the superposition of radio waves propagating along multiple paths, both direct and indirect or reflected (Roesler & Larson, 2018).

The trend present in the SNR observations is imposed by the antenna gain pattern contribution. The SNR data for each satellite can be modeled according to Eq. (1), as defined by Geremia-Nievinski (2023):

$$s(e) = A(e) \cdot \cos(4\pi\lambda^{-1} H \sin(e) + \phi(e)) \quad (1)$$

where the parameter $A$ represents the amplitude of the SNR, $e$ denotes the satellite elevation angle, $H$ is the reflector height, $\lambda$ is the carrier wave wavelength, and $\phi$ corresponds to the non-geometric interferometric phase (Nievinski & Larson, 2014). For altimetric applications, such as water level monitoring, the first and last parameters ($A$ e $\phi$) are considered practically constant over short tracking arcs. The satellite elevation is obtained from orbital ephemerides. The unknown parameter of interest in altimetry is solely the reflector height $H$. Thus, Eq. (1) can be approximated as a sinusoid, $s \approx A \cos(H\, k_z + \phi)$, using $k_z = 4\pi\lambda^{-1} \sin(e)$ as the independent variable instead of time, with the unknown $H$ assuming the role normally attributed to frequency..

# 3 METHODOLOGY

## 3.1 Study Area

Rio Grande is a municipality in the state of Rio Grande do Sul, part of the so-called Costa Doce, one of the largest lagoon complexes in the world. Located on the southern bank of the estuary connecting Patos Lagoon to the Atlantic Ocean, the National Capital of Waters (Law No. 14,746, 2023) is bounded to the north by Patos Lagoon and the municipality of Pelotas, to the south by the municipality of Santa Vitória do Palmar, to the east by the Atlantic Ocean and the Rio Grande channel, and to the west by the municipalities of Pelotas and Arroio Grande and by Lagoa Mirim (Valente, Silva, Straube, & Nascimento, 2011). This estuarine region of Patos Lagoon is unique due to its hydrodynamics and the risks associated with rising lagoon levels, which can cause flooding and require evacuation of populations living in risky areas.

Tides in this environment play a significant role in water level dynamics, sediment transport, and estuarine salinity. Although astronomical tide is one of the factors responsible for water level variation, interactions with winds, lagoon morphology, and the resistance of the inlet bar can modify the amplitude and frequency of tidal effects. This phenomenon directly impacts the local ecology, influencing biodiversity and habitats in the region.

Water level monitoring around the city is conducted by various institutions using tide gauges, including five conventional ones: Federal University of Rio Grande - Center for the Social Interaction of Young Marine Researchers (FURG/CCMAR), Portos RS and Spectrah (SSN5, Transpetro, and Praticagem), and Portos RS and SiMCosta (Molhe Sul). In addition to the conventional tide gauges, there is a GNSS-R sensor from the Federal University of Rio Grande do Sul (UFRGS), housed at CCMAR (UFRGS/CCMAR). All these sensors operate with telemetry and are distributed along the eastern coast of the city, from the downtown area to the Molhes da Barra (Figure 1).

Figure 1 – Location sketch of the study area illustrating the spatial distribution of tide gauges within the city of Rio Grande.

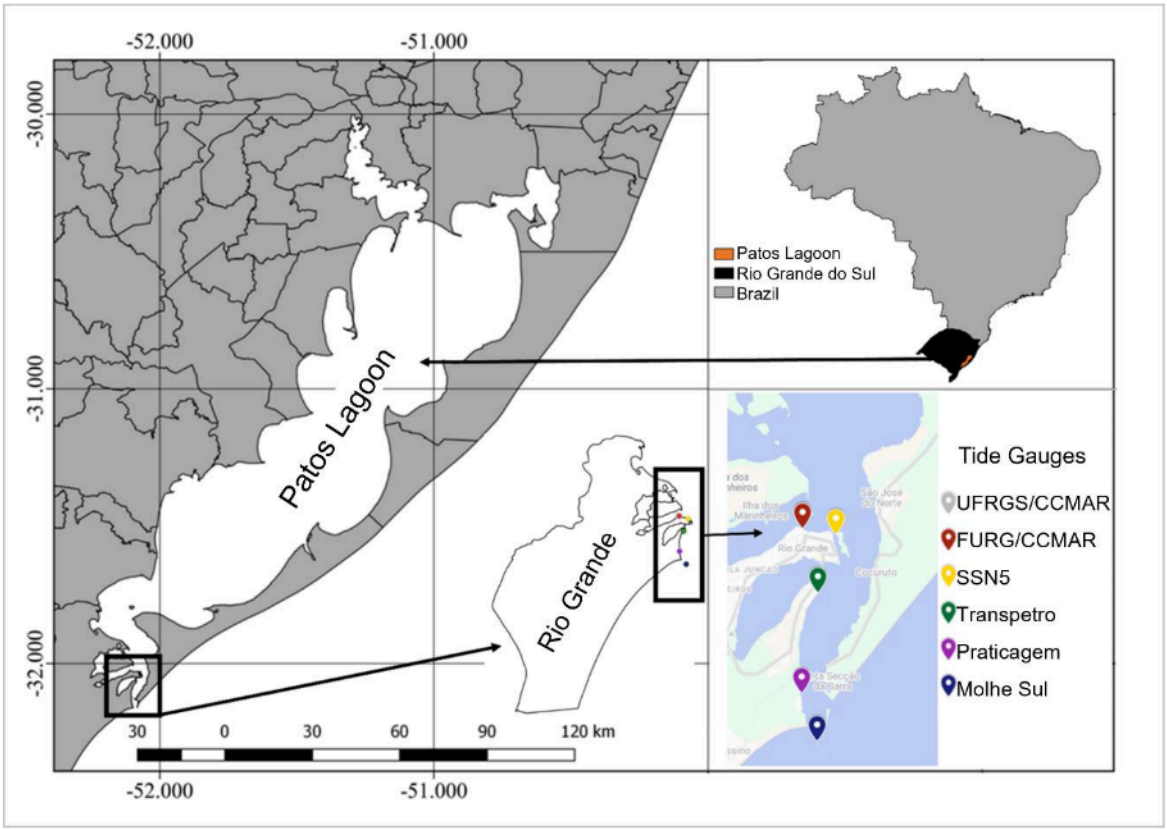


Source: The authors (2025).

## 3.2 Acquisition of Conventional Data

Initially, the sensors to be used were selected based on data availability and geographic distribution. The comparison period between the series spanned from April 1 to July 31, 2024, lasting four months and encompassing the extreme climatic event of May 2024 as well as the immediately preceding and subsequent conditions.

Data were obtained from four sources (Mario, 2023), as detailed in Table 1. The staff gauge is equipped with an attached camera, whose images are analyzed through photogrammetry (FURG, 2024). Tide gauge records were considered in their raw form, except for Molhe Sul, for which filtered data using a moving average provided by the data producer (SiMCosta) were used, resulting in a significant reduction of anomalies (outliers). Table 1 also summarizes the main characteristics of the sensors employed in the comparison of the time series. These details were critical for analyzing water behavior during the critical event. A second sensor of the hydrostatic pressure type was installed at Praticagem but was not used due to the presence of anomalous data.

### 3.2.1 GNSS-R DATA COLLECTION AND PROCESSING

The GNSS-R sensor represents a redundancy measure aimed at ensuring the continuity of the Patos Lagoon water level time series. It was installed on September 30, 2023, by UFRGS in partnership with the Rio Grande do Sul port authority, Portos RS, through the Environmental Management Program of the Port of Porto Alegre (Prestes et al., 2021). Water level data collected by this sensor, which has real-time data transmission capability via cellular network, are processed as described above and made available by TideSat (a UFRGS spin-off). These data were utilized by the Rio Grande City Hall to issue level bulletins to the population during the floods that affected Rio Grande do Sul in May 2024. Figure 2 shows the GNSS-R sensor installation site, highlighting the GNSS antenna (framed in red), positioned to ensure azimuthal coverage for reflections originating from the water.

Table 1 - Tide gauges utilized in Rio Grande (RS), including their distances relative to the GNSS-R sensor.

| | Type | Temporal Resolution (minutes) | Distance (km) | Data Access | Duration (days) |
|---|---|---|---|---|---|
| UFRGS/CCMAR | GNSS-R | 10 | 0 | TideSat (Portos RS) | 318 |
| FURG/CCMAR | Staff | 60 | 0.01 | National Water Agency | 73 |
| SSN5 | Pressure | 5 | 2.9 | Spectrah (Portos RS) | 113 |
| Transpetro | Radar | 1 | 8.0 | Spectrah (Portos RS) | 122 |
| Praticagem | Radar | 1 | 15.9 | Spectrah (Portos RS) | 183 |
| Molhe Sul | Radar | 1 | 19.7 | SiMCosta | 123 |

Prepared by: The authors (2025).

Figure 2 - Installation of the GNSS-R station in Rio Grande, highlighting the antenna (in red).

Prepared by: The authors (2025).

For real-time SNR data processing, the open-source software gnssrefl, implemented in Python (Larson, 2024) and supported by contributions from various researchers, was employed. This package facilitates the calculation and assessment of GNSS-based reflectometry parameters, enabling the retrieval of water height relative to a local reference frame. Table 2 summarizes the sensor characteristics that aided in refining the data processing.

Processing with gnssrefl begins with calculating the satellite elevations and azimuths relative to the local horizon, based on ephemerides (either broadcast or precise). Subsequently, the Fresnel reflection zones can be visualized, which indicate the region around the specular reflection point on the horizontal plane surrounding the antenna; this step is essential to exclude undesired reflectors or obstructions (Larson, Nievinski, & Freymueller, 2013).

Table 2 - Parameters used in the processing of the GNSS-R station in Rio Grande; the height is a nominal average value; the azimuthal range is clockwise.

| Parameters | Adopted Values |
|---|---|
| Ellipsoidal altitude | 10.575 m |
| Antenna height above water | 12 m |
| Constellations | GPS |
| Carrier frequency | L1 |
| Azimuthal range | 330 to 90 degrees |
| Elevation range | 5 to 30 degrees |

Prepared by: The authors (2025).

The Fresnel zones are ellipses whose dimensions are determined by the antenna height above the reflecting surface, the elevation angle between the satellite and the local horizon, and the carrier wavelength (Larson & Nievinski, 2013). Figure 3 illustrates the Fresnel zones at the UFRGS/CCMAR station, which aided in delimiting the azimuth necessary to retrieve the water height in the vicinity of the station, emphasizing the importance of discarding azimuths outside the reflection zone of interest.

The elevation range was selected considering the distance between the antenna and the water. Lower elevation angles correspond to reflections located farther away, while higher elevations correspond to reflection points closer to the antenna. In this context, to prevent the antenna from capturing reflections outside

the water, the elevation range was set between 5° and 30°, preserving water height retrievals at a horizontal distance between 15 and 102 meters from the antenna. Thus, obstructions very close to the antenna (such as the dock and anchored vessels) are excluded from reflections.

Figure 3 - Reflection zones surrounding the GNSS-R station in Rio Grande; ellipses in cyan, green, red, blue, and yellow correspond to elevations of 25°, 20°, 15°, 10°, and 5°, respectively.

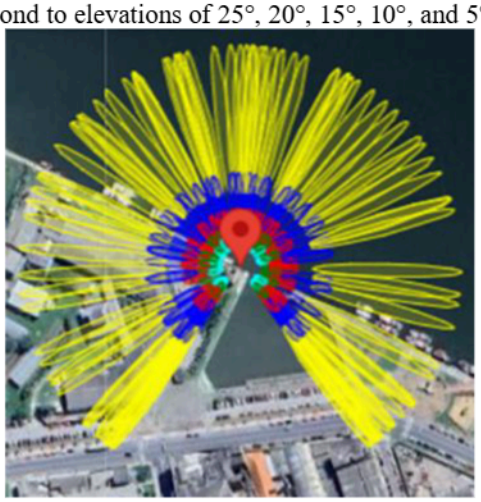

Prepared by: The authors (2025).

The gnssrefl software employs spectral analysis through the Lomb–Scargle periodogram (LSP) to extract the dominant frequency from the SNR data. Although the SNR data are sampled at regular time intervals, they are irregular in terms of satellite elevation angle, which is the independent variable in Equation (1). After determining the reflector height for each ascending or descending satellite arc, an irregularly spaced water level time series is obtained.

To regularize the altimetric sampling in time, a spline curve fitting is applied, composed of cubic polynomial segments continuously connected at specific knots (four knots per day). This fitting smooths random noise while maintaining proximity to the actual data, accounting for variations caused by reflector conditions such as tides (Purnell et al., 2020; Strandberg, Hobiger, & Haas, 2016). Following spline adjustment, the curve is evaluated every 10 minutes to generate a regularly spaced water level time series. However, it is important to note that this temporal spacing does not represent the actual temporal resolution, which is not constant in GNSS-R altimetry and varies as satellites move across the sky. In summary, the processing steps include separating GNSS satellite arcs, computing periodograms to determine dominant frequencies (related to reflector heights), and finally filtering the water height series.

## 3.3 Compatibility between sensor data

To ensure compatibility between the series, data plotting was performed to identify possible temporal or vertical shifts. The time zone was adjusted, as the FURG/CCMAR and Praticagem series were in Brasília time (UTC−3), while the other series were in GMT/UTC. Subsequently, compatibility among series referenced to different altimetric datums was established by vertically aligning them as follows: the UFRGS/CCMAR series was linearly interpolated with respect to the sampling times of each conventional series, ensuring temporal correspondence between the datasets. To preserve interpolation integrity, a tolerance of 10 minutes was set at this stage to discard sensor failure periods. Thereafter, the difference between the interpolated and original series was calculated, considering only valid points. Finally, each original series was aligned by subtracting the median difference, as summarized in Table 3. This step was necessary due to the impossibility of absolute comparison, resulting from the lack of a homogeneous topographic survey across all tide gauge stations.

Table 3 - Median altimetric difference between UFRGS/CCMAR and other tide gauges (in centimeters).

| Tide Gauge | Difference (cm) |
|---|---|
| FURG/CCMAR | 13.8 |
| SSN5 | 93.3 |
| Transpetro | 95.7 |
| Praticagem | 90.1 |
| Molhe Sul | 16.1 |

Prepared by: The authors (2025).

It is worth emphasizing that measurement conditions differ among tide gauges due to the distinct data acquisition techniques. Both the staff gauge and radar sensors provide point measurements of the water level. However, GNSS-R encompasses a broader measurement area, which is directly related to the satellite elevation angle. Consequently, data collection with the GNSS-R sensor occurs over horizontal ranges distant from the antenna, whereas the other sensors collect data at the exact point of their installation. For example, the FURG/CCMAR sensor acquires water level data at a specific setback from the pier, as illustrated in Figure 4. Given this, the differing data acquisition methods - even at nearby locations - may cause discrepancies between measurements due to local water behavior being influenced by external and site-specific effects, such as water reverberation caused by vertical structures like the pier.

Figure 4 - Location of UFRGS/CCMAR and FURG/CCMAR at Patos Lagoon, in the northern area of the city of Rio Grande.


Prepared by: The authors (2025).

## 3.4 Analysis of Water Level Dynamics

The comparison between the time series from conventional tide gauges and the GNSS-R sensor aimed to analyze water level behavior across the sensor locations during the extreme event. The analysis of water level dynamics during the 2024 flood was conducted in two stages: direct comparison of the time series and harmonic analysis of tidal constituents (Geremia-Nievinski et al., 2020).

In the direct comparative analysis, the time series were superimposed over time. To quantify the agreement between the series, the standard deviation of the differences and the coefficient of determination ($R^2$) were calculated. Finally, a scatter plot was generated. Through this approach, water dynamics were observed and compared at different locations throughout the city.

In the harmonic analysis, all tide gauge data were initially resampled or decimated to a one-hour interval, corresponding to the original sampling interval of the FURG/CCMAR sensor. Since the objective was to analyze tidal constituents with approximately 24-hour periods, the 1-hour interval was suitable for this purpose and reduced memory consumption in computing the Fourier transform. Subsequently, it was necessary to remove low-frequency water level variations caused by hydrological effects. This allowed the calculation of tidal constituents based solely on high-frequency, or short-period, oscillations that more accurately represent the astronomical forcing in hydrodynamics. To achieve this, the series was smoothed using a 7-day moving

average. The smoothed series was then subtracted from the original series, resulting in a detrended series. It is important to note that this procedure was applied to all tide gauge series.

Both temporal and harmonic analyses will aid in understanding the propagation of tidal waves and local interactions, such as the influence of wind, atmospheric pressure, and estuary geometry. Comparing tide gauges at different points along the estuary will provide insights into phase lags, local amplifications, and dissipative effects. This approach offers mechanisms to assess influences on water level variation, thereby improving coastal dynamics forecasting and management.

# 4 RESULTS AND DISCUSSION

## 4.1 Comparison of Time Series

Figure 5 presents the time series from all tide gauges. A pronounced water level rise during the extreme event, the flood wave that affected Rio Grande do Sul in May (around day 137), is clearly observable. Subsequently, each tide gauge will be compared to the UFRGS/CCMAR series, in pairs, by increasing horizontal distance (Figure 1).

Figure 5 - Time series of all tide gauges; a vertical shift of 1.5 m was applied to each series solely for improved visibility in this graph.

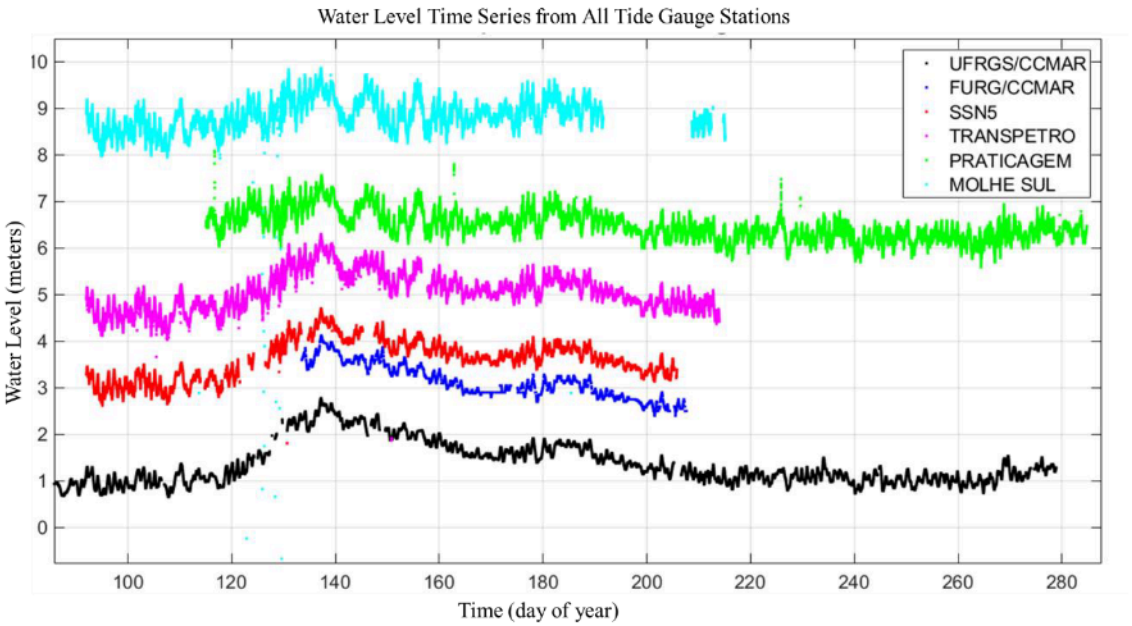


Prepared by: The authors (2025).

Figure 6(a) shows a strong similarity between water levels obtained with the UFRGS/CCMAR and FURG/CCMAR sensors, located only 10 meters apart. It also highlights that the FURG/CCMAR series was affected during the period between 168 and 172, resulting in identical data points for several hours, which can be as problematic as data loss. The UFRGS/CCMAR series also exhibited failures between days 127 and 130, with brief resumptions of measurements during that period. These results underscore the importance of data redundancy at the same location to ensure continuity of time series.

Figure 6(b) further displays the dispersion of levels obtained by the two techniques, with most points concentrated along the diagonal line, yielding a coefficient of determination of 0.99 and a standard deviation of 3.8 cm. Although the staff gauge has centimeter-level numerical resolution, its accuracy or repeatability is not specified, given the automatic photogrammetric reading procedure applied to the attached camera. The comparison result between the two techniques aligns with previous GNSS-R sensor validation performed using radar in a fluvial environment (Fagundes et al., 2021), where a standard deviation of 2.9 cm for daily averages was obtained.

Figure 6 - Time series of UFRGS/CCMAR and FURG/CCMAR (a) and scatter plot (b).

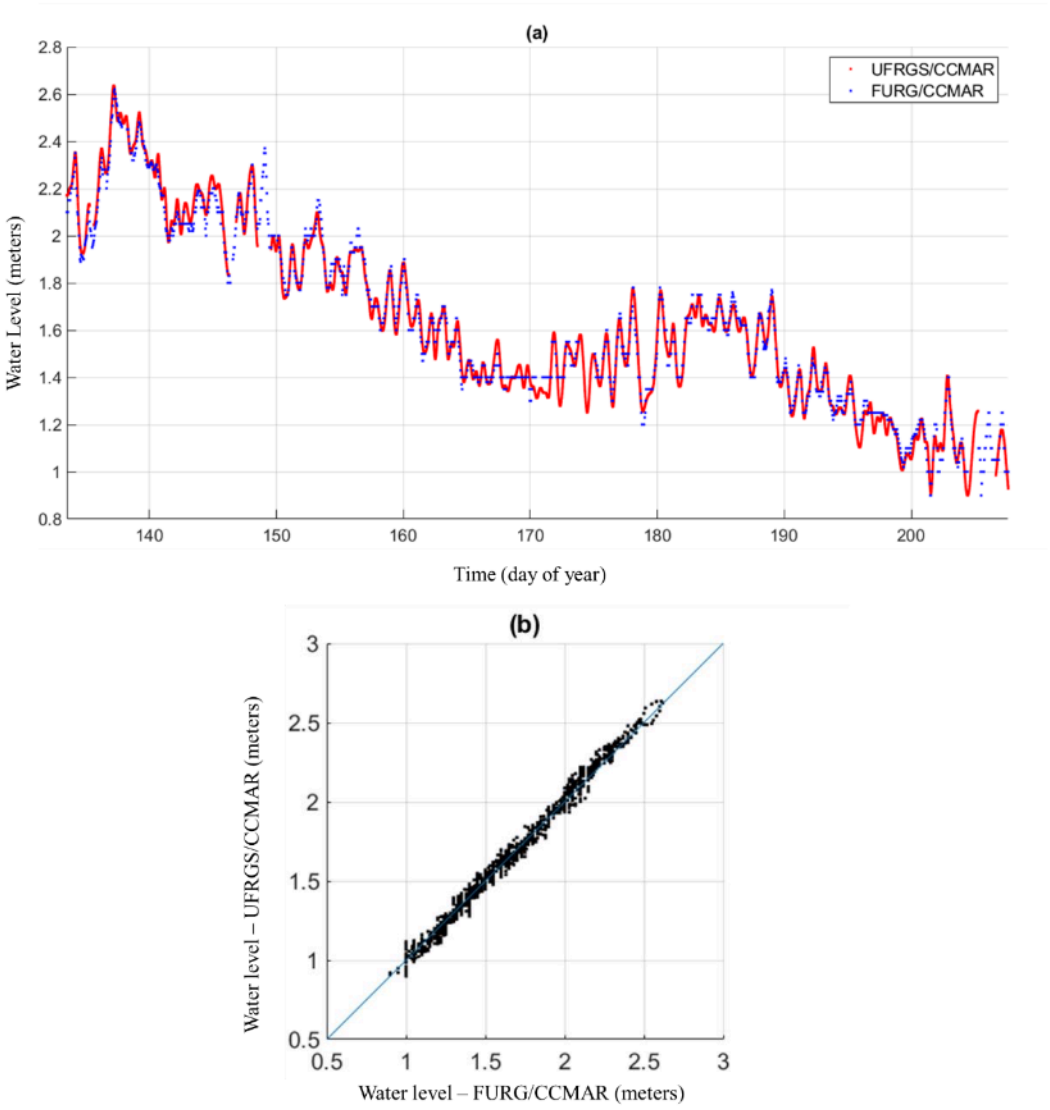


Prepared by: The authors (2025).

In the comparison between the UFRGS/CCMAR and SSN5 time series, which are separated by approximately 3 km, a good agreement was observed in late March and throughout most of April (see Fig. 7a). After this period, the conventional sensor experienced data outages on days 121–123, 124–126, and 133–134, with brief intervals of resumed operation between these gaps. The longest continuous failure occurred between days 145 and 147. The SSN5 series, sampled at 5-minute intervals, exhibited high-frequency oscillations, whereas the GNSS-R series, sampled at 10-minute intervals, presented smoother curves, with some extreme values being underestimated. These differences between peaks and troughs may be attributed to the irregular altimetric sampling in time and the subsequent smoothing introduced by the spline used in the reflectometric processing. Figure 7b shows a greater dispersion between the UFRGS/CCMAR and SSN5 datasets compared to the FURG/CCMAR dataset, indicating discrepancies arising from the spatial separation between sensors and changes in water-level dynamics.

Following a flood peak (day 137), the series diverged but subsequently realigned, indicating that the water level at UFRGS/CCMAR remained above that at SSN5 during the flood wave. This suggests that the empirical vertical alignment procedure applied to the series was adequate (Table 3). Therefore, it is proposed that a persistent water level difference exists between the two locations, influenced by the substantial hydrological discharge during the period or by wind effects. It is important to note that SSN5 is situated on a small islet adjacent to the inner coast, which may cause reflection and consequent reverberation of waves. The absence of data in both series once again highlights the importance of sensor redundancy to ensure data continuity. The coefficient of determination (0.98) and the standard deviation (9.3cm) indicated good agreement between the series. It is worth noting that the standard deviation, approaching decimeter scale,

showed a significant increase compared to the centimeter-scale value observed in the previous analysis between UFRGS/CCMAR and FURG/CCMAR.

Figure 7 - Overlaid time series of UFRGS/CCMAR and SSN5 (a) and scatter plot (b).

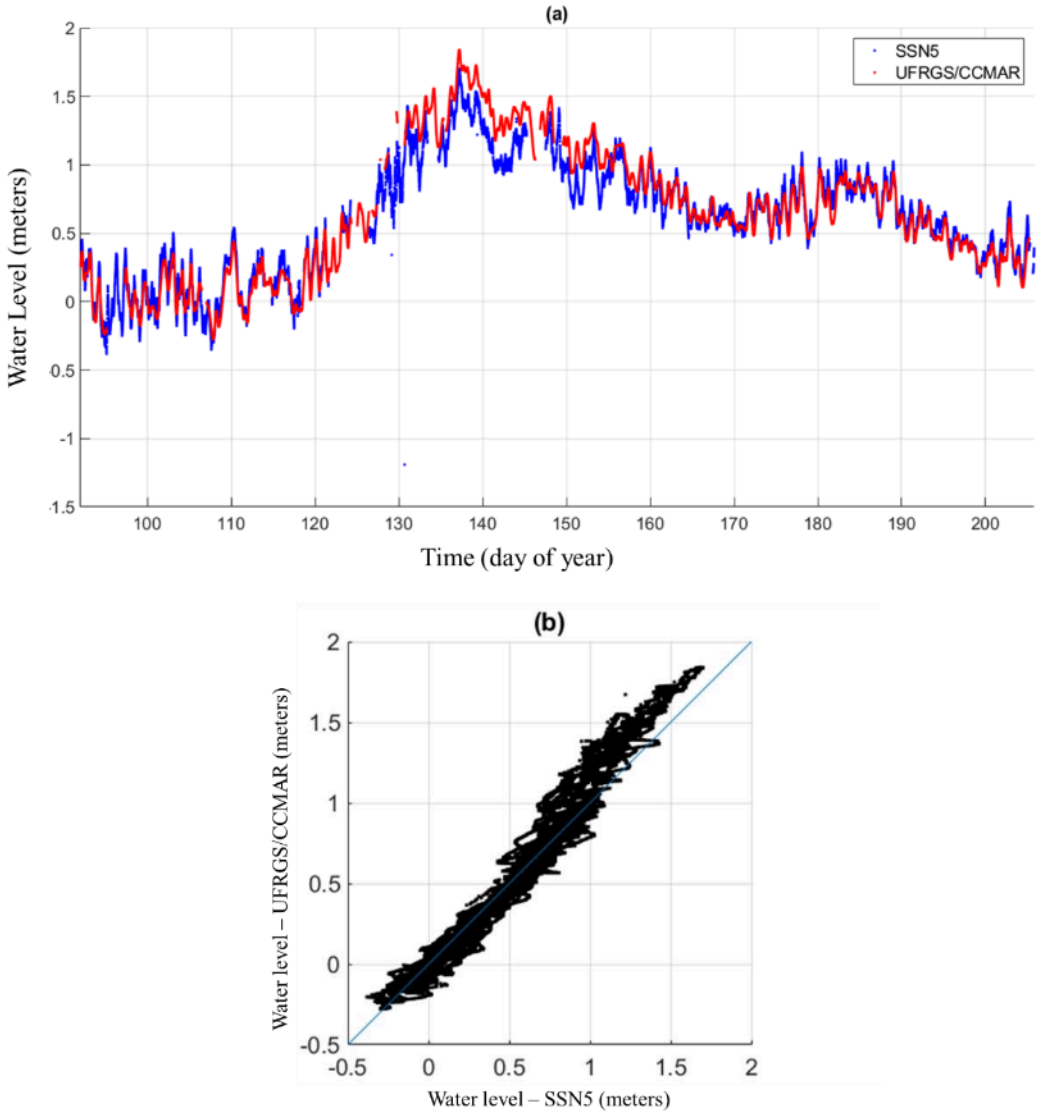


Prepared by: The authors (2025).

In the third comparison, the relationship between the UFRGS/CCMAR and Transpetro sensors, located 8 km apart, was investigated. The Transpetro sensor experienced a failure during the analyzed period, specifically between days 156 and 157. After the flood peak, the series diverged, with the Transpetro series showing a more abrupt decrease in water level. The Transpetro time series, as shown in Figure 8(a), exhibited greater variability in water level compared to the UFRGS/CCMAR series. The increased discrepancy results from the larger distance between the tide gauges and the closer proximity of the Transpetro station to the sea. The scatter plot in Figure 8(b) displays the concentration of points around the diagonal line, with a noticeable impact from some anomalous values (outliers). Metrics indicated a slightly lower coefficient of determination (0.95) and a higher standard deviation (14.5 cm) compared to the previous analysis.

Figure 8 - Overlaid time series of UFRGS/CCMAR and Transpetro (a) and scatter plot (b).

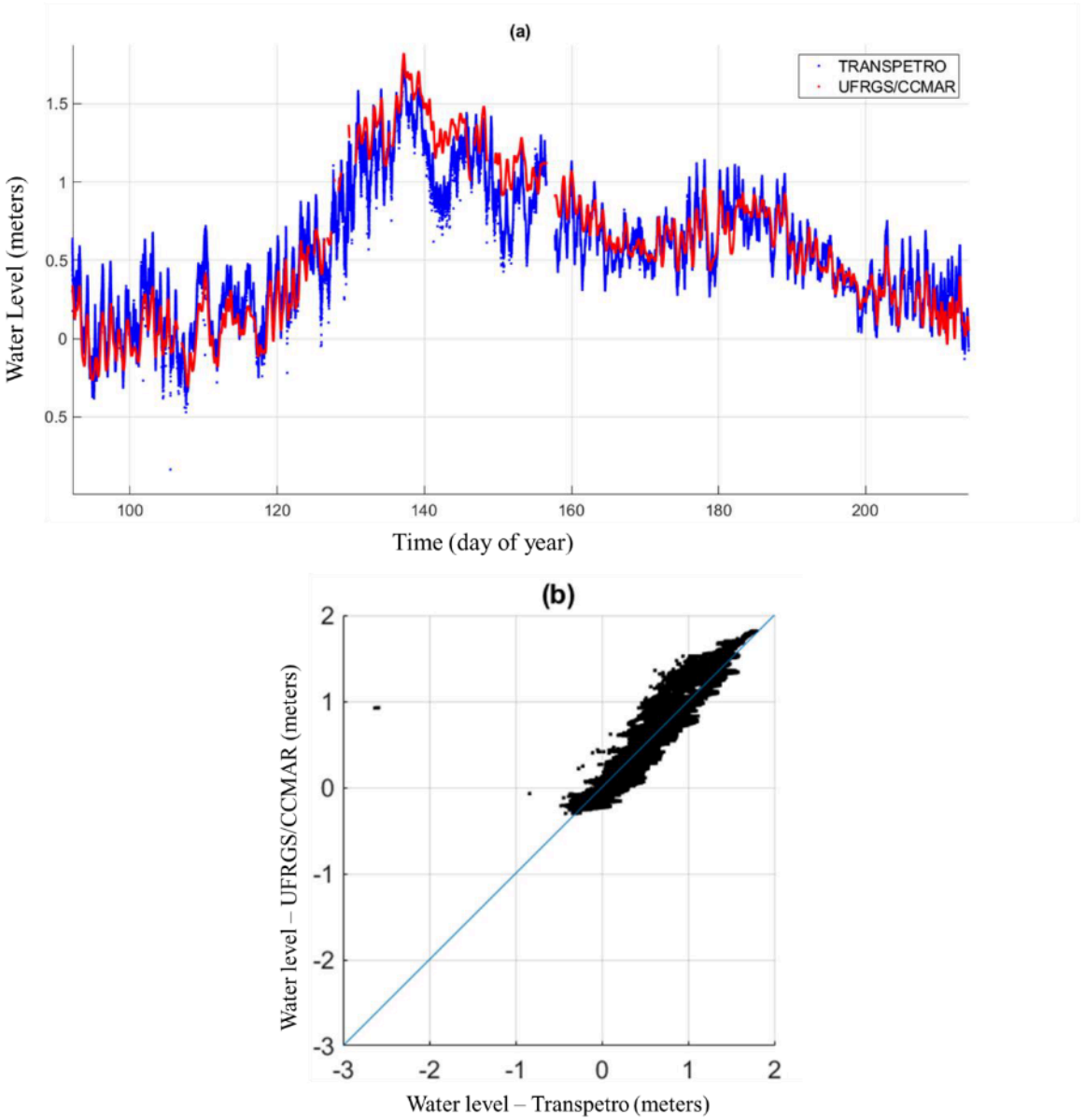


Prepared by: The authors (2025).

The GNSS-R (UFRGS/CCMAR) and Praticagem time series, located 16 km apart, exhibited lower agreement than previous analyses, with significant variations between days 120 and 160. As observed in Figure 9(a), the series showed greater absolute discrepancies during the first 50 days, possibly because of the extreme event. After day 200, discrepancies stabilized, indicating good agreement between the sensors. This post-flood period was only available in the Praticagem series and not in the other conventional tide gauges.

However, it is worth noting the greater water level variability at the Praticagem sensor location, indicating that the sensor registered larger level fluctuations. This is attributed to the local water characteristics and the sensor's temporal sampling, which allows detection of higher-frequency oscillations. Statistically, the coefficient of determination (0.78) indicated lower correspondence, and the standard deviation (22.5 cm) pointed to decimeter-scale discrepancies. The elevated standard deviation suggested high dispersion of the differences, as shown in Figure 9(b), reflecting the variability in water behavior.

The stabilization of discrepancies after the extreme event suggested that the series exhibited more consistent and correlated measurements over time, although this remains the most discrepant comparison relative to the previous analyses. Anomalous values are also present, visible both in the scatter plot and the time series near days 120, 160, and 230. These positive anomalies in the Praticagem series suggest they may be caused by transient obstructions between the radar and the water.

Figure 9 - Overlaid time series of UFRGS/CCMAR and Praticagem (a) and scatter plot (b).

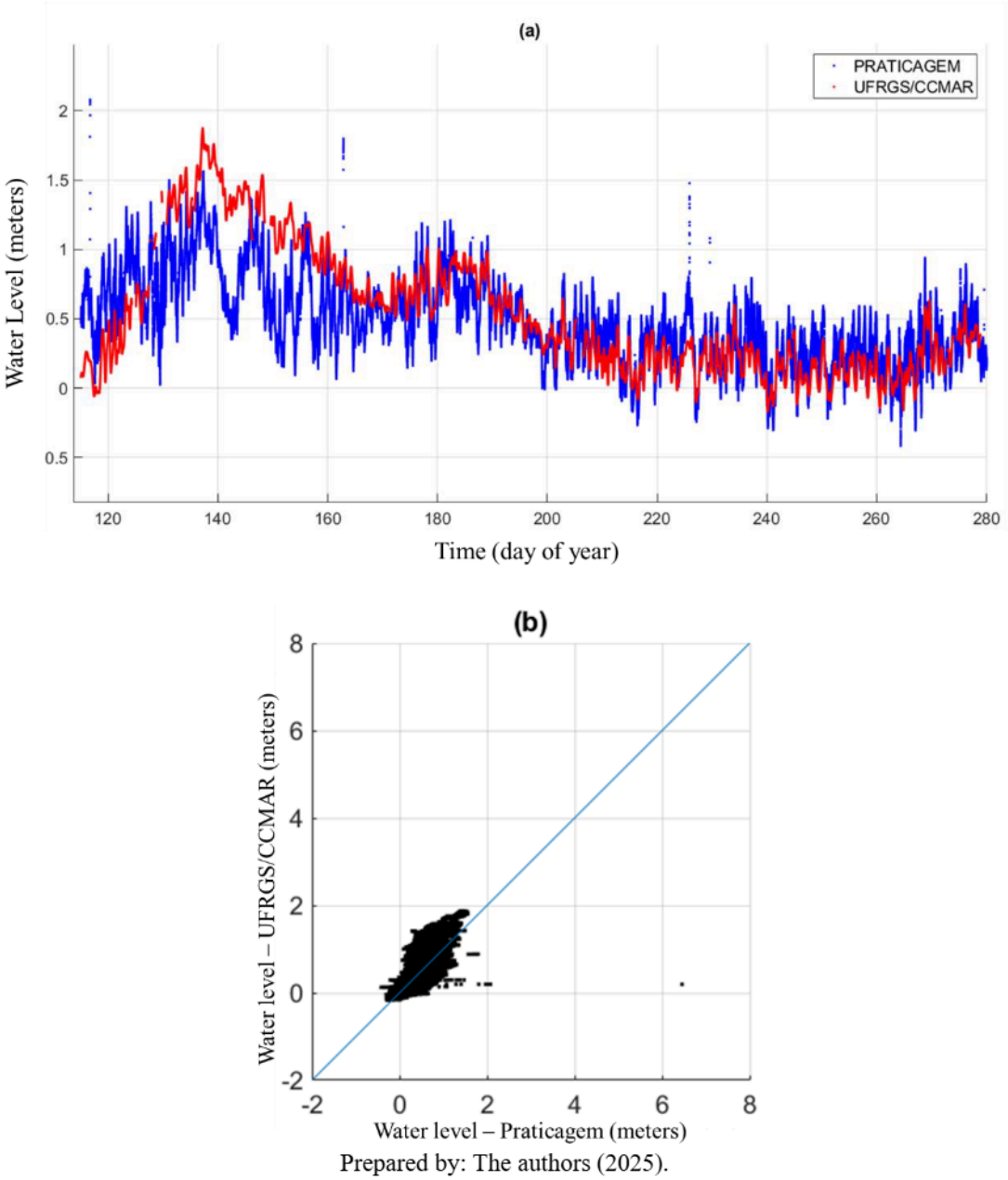


Prepared by: The authors (2025).

Figure 10 shows the time series from UFRGS/CCMAR and Molhe Sul, located 20 km apart. A pronounced discrepancy is evident, with greater water level variability in the Molhe Sul region. This analysis revealed the lowest coefficient of determination (0.62) among all comparisons. The scatter plot, shown in Figure 10(b), indicates a high level of noise. This suggests that water dynamics differ significantly between the two locations. The standard deviation of 35.5 cm highlights substantial discrepancies between the series, particularly near day 140. These results were expected since the Molhe Sul sensor, located offshore, is subject to a different dynamic environment than the UFRGS/CCMAR tide gauge, which affects measurements and complicates comparison.

Figure 10 - Overlaid time series of UFRGS/CCMAR and Molhe Sul (a) and scatter plot (b).

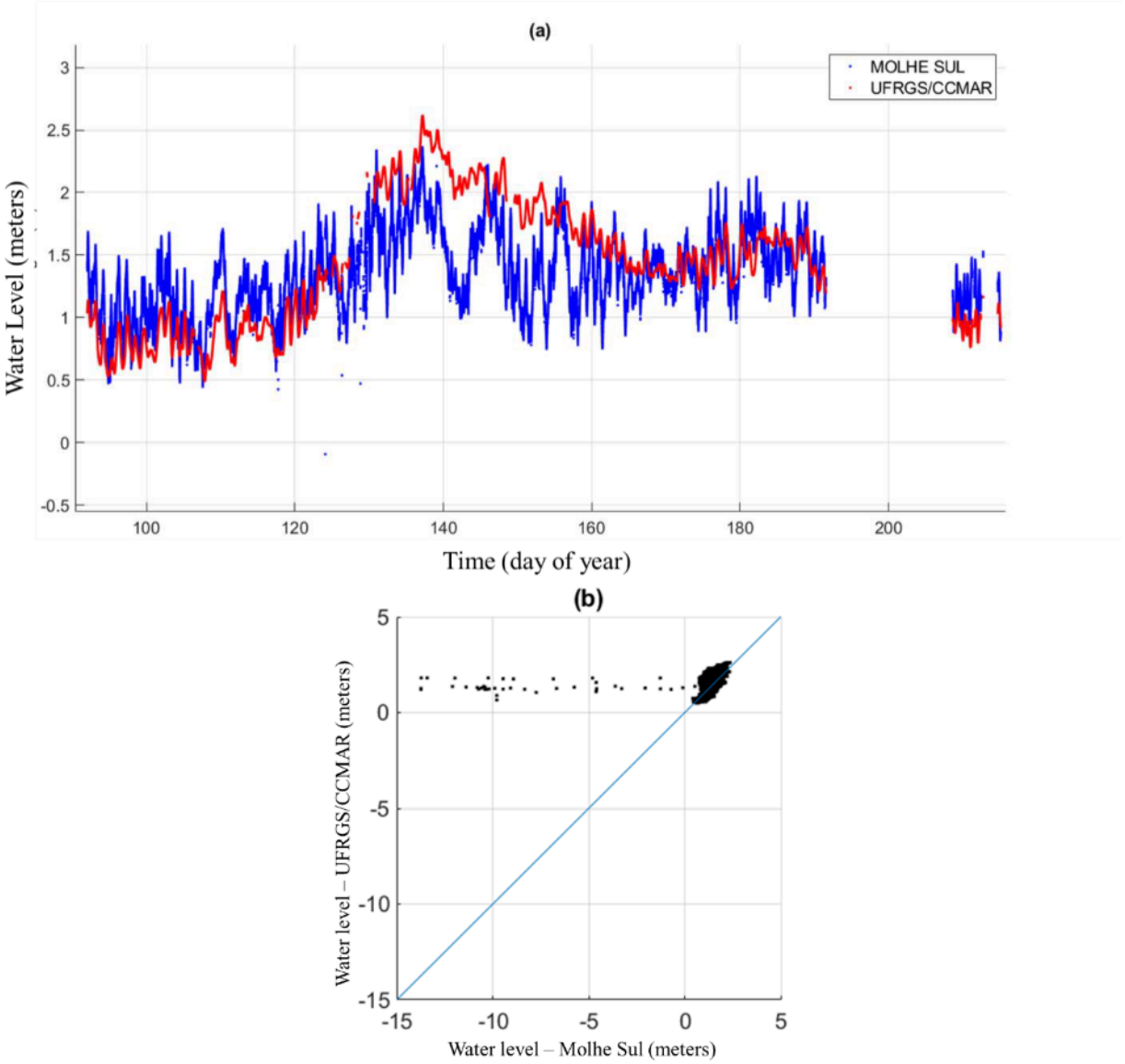


Prepared by: The authors (2025).

### 4.1.1 DISCUSSION OF TEMPORAL RESULTS

Comparisons between the GNSS-R site and conventional sensors indicated agreement approximately inversely proportional to the distance, but with variations depending on location and measurement conditions. As the distance between sensors increased, the coefficient of determination decreased while the standard deviation increased, as shown in Figure 11. The largest absolute discrepancies tended to occur during the flood peak (day 140). Comparison between coincident stations exhibited centimeter-level differences, reinforcing the relative accuracy between the GNSS-R and staff gauge (with camera) techniques, despite occasional sensor failures.

The comparison with SSN5 showed greater dispersion and a lower coefficient of determination than the comparison with FURG/CCMAR. The shorter temporal spacing of SSN5 captured high-frequency oscillations not recorded by GNSS-R; nevertheless, the series yielded an excellent coefficient of determination. After a flood peak, the series diverged for a period, reflecting different responses to water level variation at distinct locations. The Transpetro series exhibited dispersion immediately after the flood wave caused by the extreme event, with the sensor registering a faster decline in water level. The Praticagem sensor demonstrated lower agreement with GNSS-R after the extreme event compared to previous analyses. Observing the overlapped time series plot reveals greater water variability in the Transpetro region, resulting in higher discrepancies. The greatest divergence was observed at Molhe Sul, evidencing significant differences in water dynamics relative to the GNSS-R sensor, due to the tide gauge's location at the Molhes da Barra, collecting

sea data. These results highlighted the influence of local hydrodynamics on measurements and the importance of multiple sensors to ensure data continuity and reliability at different points throughout the city.

.

Figure 11 - Statistics between UFRGS/CCMAR and other tide gauges: (a) standard deviation and (b) coefficient of determination. ($R^2$).

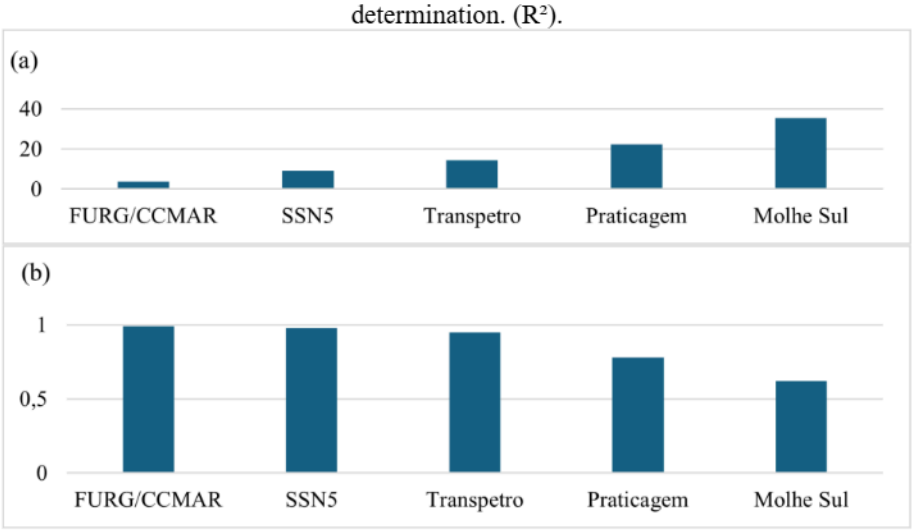


Prepared by: The authors (2025).

## 4.2 Comparison of Tidal Constituents

Figure 12 shows the flood wave removal plot for the GNSS-R sensor. It is evident that the application of a 7-day moving average was sufficient to remove the trend from the original series, leaving only high-frequency oscillations resulting from astronomical and meteorological forcings.

Figure 12 - Flood wave removal plot. Original time series (blue), 7-day moving average (red), and detrended result (black).

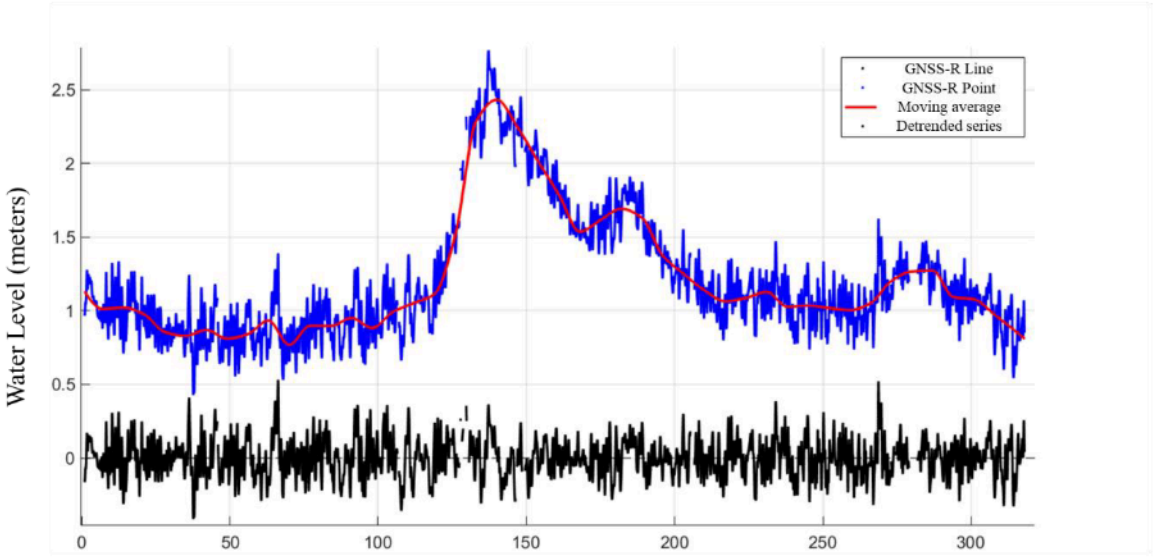


Prepared by: The authors (2025).

Table 4 presents the results for statistically significant tidal constituents: lunisolar diurnal (K1; period $T = 23.9$ h) e lunar diurnal (O1; $T = 25.8$ h) at each tide gauge. For K1, the FURG/CCMAR staff gauge exhibits the smallest amplitude difference relative to the UFRGS/CCMAR sensor, which is expected given the proximity of the stations. However, the phase analysis of K1 reveals a difference of approximately 13 degrees between UFRGS/CCMAR and FURG/CCMAR. Consequently, the vector difference was also affected. The differences observed in K1 and O1 can be attributed to various factors, including the relatively short duration of the series, measurement techniques, and interactions between the tidal wave and local features such as

estuary boundaries and artificial structures. These discrepancies aid in understanding local effects on tidal wave propagation and highlight the importance of selecting appropriate filtering methods and time series adjustments in tidal analysis.

Table 4 - Tidal constituent results for O1 and K1, showing amplitude (Amp) and phase for each tide gauge.

| **Constituent** | | **UFRGS/CCMAR** | **FURG/CCMAR** | **SSN5** | **Transpetro** | **Praticagem** | **Molhe Sul** |
|---|---|---|---|---|---|---|---|
| Symbol | Period (h) | Amp. (cm)<br>Phase (°) | Amp. (cm)<br>Phase (°) | Amp. (cm)<br>Phase (°) | Amp. (cm)<br>Phase (°) | Amp. (cm)<br>Phase (°) | Amp. (cm)<br>Phase (°) |
| K1 | 23,9 | 3.6<br>175.2 | 3.2<br>161.5 | 4.3<br>180.0 | 4.1<br>177.7 | 4.9<br>138.8 | 6.9<br>199.0 |
| O1 | 25,8 | 7.8<br>126.8 | 5.8<br>132.7 | 8.6<br>140.8 | 9.7<br>147.9 | 12.5<br>113.7 | 13.9<br>161.4 |

Prepared by: The authors (2025).

Descriptions of Tables 5 and 6 detail comparisons of phase and amplitude between different tide gauges relative to the reference UFRGS/CCMAR gauge, focusing on constituents K1 and O1. To enhance understanding and facilitate visual analysis of numerical results, it is noted that the vector difference suggests a combination of systematic effects and possibly local interferences impacting the tidal wave. Small individual differences in amplitude and phase may combine nonlinearly, amplifying the total vector difference. This occurs because the total error is influenced by phase-shifted vectors, not solely by their magnitudes.

Table 5 - Metrics for the K1 tidal constituent relative to the UFRGS/CCMAR station.

| | **Duration of Time Series (days)** | **Amplitude Difference (cm)** | **Relative Amplitude Difference (%)** | **Phase Difference (degrees)** | **Relative Phase Difference (%)** | **Combined Vector Difference (cm)** | **Relative Vector Difference (%)** |
|---|---|---|---|---|---|---|---|
| FURG | 73 | +0.4 | +9.9 | +13.7 | +3.8 | 0.9 | 24.7 |
| SSN5 | 113 | -0.7 | -20.1 | -4.8 | -1.3 | 0.8 | 22.1 |
| Transpetro | 122 | -0.6 | -16.5 | -2.5 | -0.7 | 0.6 | 17.2 |
| Praticagem | 163 | -1.4 | -38.3 | +36.4 | +10.1 | 2.9 | 82.8 |
| Molhe Sul | 99 | -3.3 | -93.7 | -23.9 | -6.6 | 3.9 | 109.9 |

Prepared by: The authors (2025).

Table 6 - Metrics for the O1 tidal constituent relative to the UFRGS/CCMAR station.

| | **Duration of Time Series (days)** | **Amplitude Difference (cm)** | **Relative Amplitude Difference (%)** | **Phase Difference (degrees)** | **Relative Phase Difference (%)** | **Combined Vector Difference (cm)** | **Relative Vector Difference (%)** |
|---|---|---|---|---|---|---|---|
| FURG | 73 | +1.9 | +24.8 | -5.9 | -1.6 | 2.0 | 26.4 |
| SSN5 | 113 | -0.8 | -10.8 | -14.0 | -3.9 | 2.2 | 27.8 |
| Transpetro | 122 | -1.9 | -25 | -21.1 | -5.9 | 3.7 | 47.9 |
| Praticagem | 163 | -4.7 | -60.7 | +13.1 | +3.6 | 5.2 | 67.2 |
| Molhe Sul | 99 | -6.1 | -79.3 | -34.5 | -9.6 | 8.7 | 112.3 |

Prepared by: The authors (2025).

### 4.2.1 DISCUSSION OF TIDAL CONSTITUENTS

The tidal behavior during the extreme event reflects the complexity of hydrodynamic interactions between the estuary and the sea, with significant influence from winds and river discharge. Notably, there is a phase difference sign inversion for the Praticagem series, which is speculated to be due to the extended post-flood period with data available for this station, compared to the other conventional tide gauges. Molhe Sul, located closer to the outlet of Patos Lagoon, exhibits a phase lag for the K1 and O1 constituents. This lag can be explained by effects such as tidal wave reflection and interaction with meteorological forcings. The hydrological discharge and winds may have directed the water flow, resulting in additional resistance to the tidal flow.

In this context, tidal amplitude appears spatially reduced in the more inland regions of the estuary,

which is expected regardless of the flood wave but may have been intensified due to the increased water level. Regarding amplitude, it was observed that only the wave recorded at the FURG/CCMAR station exhibited values lower than those at UFRGS/CCMAR, resulting in a positive difference for both O1 and K1. In all other analyses, the amplitude was higher at the other locations compared to UFRGS/CCMAR.

The O1 analyses show that the tide gauges farther from UFRGS/CCMAR exhibit greater relative vector differences. This disparity can be explained by factors such as estuary morphology, data collection technique, and even the impact of the extreme event. For K1, the relative vector difference was significantly higher at the two most distant tide gauges (Praticagem and Molhe Sul), but it does not follow a linear trend among FURG, SSN5, and Transpetro. Among these stations compared to UFRGS/CCMAR, the Transpetro station showed the lowest relative vector difference, followed by SSN5 and FURG/CCMAR.

It can be inferred that the relative vector difference of K1 decreased with the increasing duration of the time series at the three stations closest to UFRGS/CCMAR. This highlights the complexity of analyzing local water behavior, indicating that components with different periods are affected differently by linear and nonlinear factors.

## 5 CONCLUSIONS AND FUTURE WORKS

Conventional water level measurement technologies face challenges related to their installation and maintenance. In this context, the technique of navigation satellite reflectometry (GNSS-R) offers an alternative for water level monitoring, especially during extreme events, due to its advantage of enabling remote sensing measurements. In this study, we investigated the water level dynamics in the Rio Grande estuary (RS) adjacent to Patos Lagoon during the May 2024 flood event. All conventional tide gauges and the GNSS-R sensor available in the region with accessible data were employed.

The temporal comparison between pairs of tide gauges showed that the greater the distance between sensors, the more the relative water dynamics are altered, confirming initial expectations. Statistical analyses revealed that the more distant sensors, such as Molhe Sul, exhibited higher variability in results, possibly due to greater influence from astronomical and meteorological forcings.

Harmonic analysis demonstrated that tidal wave energy can propagate through different paths, resulting in phase shifts or delays. This can impact tidal amplitude and harmonic phase calculations, especially for constituents with longer periods. Phase analysis also revealed that proximity between tide gauges is not the sole determinant of observed discrepancies, with local hydrodynamic conditions being a relevant factor. The study of amplitude and phase differences for each constituent, particularly between the UFRGS/CCMAR gauge and others, provided important insights into local sensor characteristics and the influence of proximity to the sea and artificial structures.

Moreover, redundant installation of multiple sensors at the same site proved essential to ensure continuity of measurements in the event of sensor failure. This demonstrated that GNSS reflectometry for tide gauging is a viable technique when compared to conventional methods, allowing the time series to be maintained during extreme climatic events. However, further research is needed to improve its accuracy relative to the nominal precision of radar sensors. It is also noteworthy that conventional sensor data exhibited anomalies.

We recommend installing additional sensors in adjacent locations, as variations were significant from point to point. This is especially valid in environments like the Patos Lagoon estuary, where topography, bathymetry, and other local factors influence tidal behavior. Additionally, deploying sensors in currently unmonitored locations would contribute to broader spatial coverage.

Recently, the GNSS-R sensor was upgraded to include tracking of the Russian GLONASS constellation. It is recommended to investigate the impact of multi-GNSS capability, particularly on the temporal resolution of altimetric measurements. It is also suggested to analyze the impact of corrections for vertical water velocity (Larson, Nievinski, & Freymueller, 2013), which are usually negligible in environments with small tidal ranges, especially during periods of abrupt water level variation.

A longer-term tidal analysis is suggested, ideally over the same interval for all tide gauges, to enable more precise and consistent estimation of astronomical constituents at each station. The uncertainty of the

constituents should also be considered to evaluate whether differences are significant or negligible. An analysis of other stations in Patos Lagoon, outside the Rio Grande estuary, is also expected to provide information on the flood wave. Tidal analysis outside the flood period will help assess which spatial variations are persistent and the influence of the flood itself.

Finally, we recommend conducting a topogeodetic survey to calibrate the hydrographic zero levels of all tide gauges to verify bias or mean discrepancy among measurements at different stations. This would help ensure the accuracy of relative measurements and enable inference of the water surface slope, which is essential for adequate monitoring of water level dynamics in the estuary.

**Acknowledgments**

To the Graduate Program in Remote Sensing at the Federal University of Rio Grande do Sul (PPGSR/UFRGS). To Portos RS for providing the data from conventional tide gauges installed in Rio Grande. To TideSat, for providing the data obtained with the GNSS-R tide gauge during 2024 extreme event.

**Authors' Contributions**

Conceptualization: Fagundes, M. A. R e Geremia-Nievinski, F; Curadoria dos Dados: Fagundes, M. A. R; Análise Formal e Investigação: Fagundes, M. A. R e Geremia-Nievinski, F. Methodology: Geremia-Nievinski, F; Supervision: Geremia-Nievinski, F; Writing – original draft: Fagundes, M. A. R; Writing – review & editing: Fagundes, M. A. R e Geremia-Nievinski, F.

**Conflict of Interest**

The authors declare no conflict of interest.

## References

*Lei n° 14.746, de 5 de dezembro de 2023*. (2023). Confere o título de Capital Nacional das Águas ao Município de Rio Grande, no Estado do Rio Grande do Sul. https://www.planalto.gov.br/ccivil_03/_ato2023-2026/2023/lei/L14746.htm

Carrillo, D. P. (2024). Medição emergencial nível do Guaíba durante enchente de 2024—Parte 2 (Informação técnica 21; p. 2). Secretaria Estadual do Meio Ambiente e Infraestrutura, Governo do Estado do Rio Grande do Sul.

Fagundes, M. A. R., Mendonça-Tinti, I., Iescheck, A. L., Akos, D. M., & Geremia-Nievinski, F. (2021). An open-source low-cost sensor for SNR-based GNSS reflectometry: Design and long-term validation towards sea level altimetry. *GPS Solutions*. *25*(2), 73 https://doi.org/10.1007/s10291-021-01087-1

Fagundes, M. A. R., Yamawaki, M. K., Almeida, J., V. H., Leipelt, D. B., Tinti, I. M., & Geremia-Nievinski, F. (2021). TideSat - uma startup de sensoriamento remoto geodésico. *X Seminário Anual de Pesquisas em Geodésia da UFRGS–2021*, 24–28. http://hdl.handle.net/10183/231112

Geremia-Nievinski, F., Hobiger, T., Rüdiger Haas, Wei Liu, Joakim Strandberg, Sajad Tabibi, Sibylle Vey, Jens Wickert, & Simon Williams. (2020). SNR-based GNSS reflectometry for coastal sea-level altimetry – Results from the first IAG inter-comparison campaign. *Journal of Geodesy*. *94*(8), 70. https://doi.org/10.1007/s00190-020-01387-3

Geremia-Nievinski, F. (2023). Low-Cost Ground-Based GNSS Reflectometry. In M. G. Sideris (Ed.), *Encyclopedia of Geodesy* (pp. 1–5). Springer. https://doi.org/10.1007/978-3-319-02370-0_175

Geremia Nievinski, F., Toldo, E., Puhl, E., MANICA, R., Rodrigues Nunes, J. C., Fick, C., Scottá, F., & Silva da Silva, T. (2024). *Aferição emergencial da medição do nível da água durante a cheia de 2024 em Porto Alegre*. [Nota técnica] Programa de Gestão Ambiental do Porto de Porto Alegre; Portos RS e Universidade Federal do Rio Grande do Sul. Porto Alegre. https://doi.org/10.5281/ZENODO.14526745

Holden, L. D., & Larson, K. M. (2021). Ten years of Lake Taupō surface height estimates using the GNSS interferometric reflectometry. *Journal of Geodesy*, *95*(7), 74. https://doi.org/10.1007/s00190-021-01523-7

Intergovernmental Oceanographic Commission [IOC]. (2006). *Manual on sea-level measurements and interpretation – Volume IV: An update to 2006* (IOC Manuals and Guides No. 14, Vol. IV; JCOMM Technical Report No. 31; WMO/TD No. 1339). UNESCO. https://psmsl.org/train_and_info/training/manuals/manual_14_final_21_09_06.pdf

Larson, K. M. (2016). GPS interferometric reflectometry: Applications to surface soil moisture, snow depth, and vegetation water content in the western United States. *Wiley Interdisciplinary Reviews: Water*, *3*(6), 775–787. https://doi.org/10.1002/wat2.1167

Larson, K. M. (2024). Gnssrefl: An open source software package in python for GNSS interferometric reflectometry applications. *GPS Solutions*, *28*(4), 165. https://doi.org/10.1007/s10291-024-01694-8

Larson, K. M., & Nievinski, F. G. (2013). GPS snow sensing: Results from the EarthScope Plate Boundary Observatory. *GPS Solutions*, *17*(1), 41–52. https://doi.org/10.1007/s10291-012-0259-7

Larson, K. M., Ray, R. D., Nievinski, F. G., & Freymueller, J. T. (2013). The accidental tide gauge: A GPS reflection case study from Kachemak Bay, Alaska. *IEEE Geoscience and Remote Sensing Letters*, *10*(5), 1200–1204. https://doi.org/10.1109/LGRS.2012.2236075

Larson, K. M., Ray, R. D., & Williams, S. D. P. (2017). A 10-Year Comparison of Water Levels Measured with a Geodetic GPS Receiver versus a Conventional Tide Gauge. *Journal of Atmospheric and Oceanic Technology*, *34*(2), 295–307. https://doi.org/10.1175/JTECH-D-16-0101.1

Marcuzzo, F. F. N., Kenup, R. E., Zanetti, H. P., Benvenutti, L., Oliveira, M. P. de, Wilson, E. da S., Acosta, C. C., & Bao, R. (2024). *Aferição direta e avalição indireta do nível máximo de rios em estações fluviométricas e marcas de inundação no Rio Grande do Sul na grande cheia de maio de 2024*: 9. Versão (p. 63) [Nota técnica]. Serviço Geológico do Brasil. https://rigeo.sgb.gov.br/handle/doc/24939.11

Mario, H. F. de S. (2023). Levantamento hidrográfico do Porto de Rio Grande - pedido de medição de 10 de março de 2023. (Serviços de batimetria realizados para atendimento do contrato RG.1206/22 Porto de Rio Grande) [Relatório técnico]. Spectrah Oceanografia e Meio Ambiente.

Marques, W. C., & Möller, O. O. (2008). Variabilidade temporal em longo período da descarga fluvial e níveis de água da Patos Lagoon, Rio Grande do Sul, Brasil. *Revista Brasileira de Recursos Hídricos 13*(3), 155–163. https://doi.org/ 10.21168/rbrh.v13n3.p155-163

Míguez, B. M., Testut, L., & Wöppelmann, G. (2012). Performance of modern tide gauges: Towards mm-level accuracy. *Scientia Marina, 76*(S1), 221–228. https://doi.org/10.3989/scimar.03618.18A

Nievinski, F. G., & Larson, K. M. (2014). Forward modeling of GPS multipath for near-surface reflectometry and positioning applications. *GPS Solutions, 18*(2), 309–322. https://doi.org/10.1007/s10291-013-0331-y

Nogueira, R. M. (2006). Aspectos hidrodinâmicos da Patos Lagoon na formação do depósito lamítico ao largo da praia de Cassino – RS [Dissertação de Mestrado em Engenharia Oceânica, Universidade Federal do Rio de Janeiro. https://w1files.solucaoatrio.net.br/atrio/ufrj-peno_upl//THESIS/10001728/2006_mestrado_raphael_miguez_nogueira_20210819151712523.pdf

Oliveira, M. P. (2008). Análise dos parâmetros meteorológicos e oceanográficos de um evento de maré meteorológica ocorrido em Tramandaí—Rio Grande do Sul [Trabalho de Conclusão de curso - Graduação em Geografia, Universidade Federal do Rio Grande do Sul]. https://lume.ufrgs.br/handle/10183/17346

Permanent Service for Mean Sea Level (PSMSL). (2019). *Report of the PSMSL and GLOSS Group of Experts meeting XVI* (PSMSL Report No. 3). National Oceanography Centre. https://psmsl.org/about_us/other_reports/PSMSL_GE-GLOSS_XVI_2019.pdf

Prestes, L. D., Silva, T. S. da., Brentano, T. B., Aquino, N. de., Filgueras, A. S., Oliveira, M. A. de., Ruiz, A. C., Silva, D. F. da., Sfredo, G. A. e Onetti, J. G. (2021). Gestão ambiental no porto de Porto Alegre, Sul do Brasil: uma abordagem ecossistêmica. 2023. *X Congresso sobre Planejamento e Gestão de Zonas Costeiras dos Países de Expressão Portuguesa,* Rio de Janeiro. Disponível em:

https://www.researchgate.net/publication/358265711

Purnell, D., Gomez, N., Chan, N. H., Strandberg, J., Holland, D. M., & Hobiger, T. (2020). Quantifying the Uncertainty in Ground-Based GNSS-Reflectometry Sea Level Measurements. *IEEE Journal of Selected Topics in Applied Earth Observations and Remote Sensing*, *13*, 4419–4428.

Purnell, D., Gomez, N., Minarik, W., & Langston, G. (2024). Real-Time Water Levels Using GNSS-IR: A Potential Tool for Flood Monitoring. *Geophysical Research Letters, 51*(5), e2023GL105039. https://doi.org/10.1029/2023GL105039

Roesler, C., & Larson, K. M. (2018). Software tools for GNSS interferometric reflectometry (GNSS-IR). *GPS Solutions, 22*(3). https://doi.org/10.1007/s10291-018-0744-8

Strandberg, J., Hobiger, T., & Haas, R. (2016). Improving GNSS-R sea level determination through inverse modeling of SNR data. *Radio Science, 51*(8), 1286–1296. https://doi.org/10.1002/2016RS006057

Torres, L. H. (2012). Águas de maio: a enchente de 1941 em Rio Grande. *Historiae (Rio Grande)*, *3*(3), p. 239-254. Disponível em: https://biblat.unam.mx/es/revista/historiae-rio-grande/2.

Universidade Federal do Rio Grande - FURG. (2024). FURG disponibiliza transmissão do nível da Patos Lagoon em tempo real. https://www.furg.br/noticias/noticias-institucional/furg-disponibiliza-transmissao-do-nivel-da-lagoa-dos-patos-em-tempo-real.

Valente, R. de M., Silva, J. M. C. da, Straube, F. C., & Nascimento, J. L. X. do. (2011). *Conservação de Aves Migratórias Neárticas no Brasil* (1ª ed., Vol. 1), Conservação Internacional.

## Biography of the Principal Author

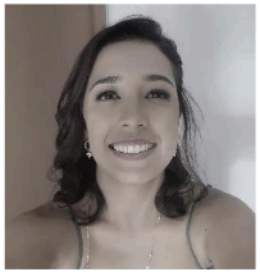

Manuella Anaís Rodrigues Fagundes is a Cartographic Engineer and Ph.D. in Remote Sensing and Geoprocessing from Federal University of Rio Grande do Sul, Porto Alegre, RS, Brazil. She is currently an Assistant Professor at the Federal University of Recife, PE, Brazil. Her research interests include GNSS Reflectometry (GNSS-R) and Cartography.